QUANTUM CASCADE LASER: APPLICATIONS IN CHEMICAL DETECTION AND ENVIRONMENTAL MONITORING

by

Jelena RADOVANOVIĆ and Vitomir MILANOVIĆ

Received on June 24, 2009; accepted in revised form on July 17, 2009

In this paper we consider the structural parameter optimization of the active region of a GaAs-based quantum cascade laser in order to maximize the optical gain of the laser at the characteristic wavelengths, which are best suited for detection of pollutant gasses, such as SO_2, HNO_3, CH_4, and NH_3, in the ambient air by means of direct absorption. The procedure relies on applying elaborate tools for global optimization, such as the genetic algorithm. One of the important goals is to extend the applicability of a single active region design to the detection of several compounds absorbing at close wavelengths, and this is achieved by introducing a strong external magnetic field perpendicularly to the epitaxial layers. The field causes two-dimensional continuous energy subbands to split into the series of discrete Landau levels. Since the arrangement of Landau levels depends strongly on the magnitude of the magnetic field, this enables one to control the population inversion in the active region, and hence the optical gain. Furthermore, strong effects of band non-parabolicity result in subtle changes of the lasing wavelength at magnetic fields which maximize the gain, thus providing a path for fine-tuning of the output radiation properties and changing the target compound for detection. The numerical results are presented for quantum cascade laser structures designed to emit at specified wavelengths in the mid-infrared part of the spectrum.

Key words: quantum cascade laser, electron-phonon interactions, electronic structure, global optimization, intersubband transitions

INTRODUCTION

Quantum cascade laser (QCL) is a relatively new type of unipolar multilayered semiconductor source, based on electronic transitions between confined states created in the conduction band with the alternate growth of well and barrier materials, which can be fabricated to operate in the mid and far-infrared spectral range [1, 2]. Its emission wavelength can be tuned by the design of the band structure, and so far, "tailoring" of the active band profile has allowed reaching laser wavelengths from 3 μm up to 250 μm. The accuracy in the band design requires material growth by molecular beam epitaxy, which provides thickness control down to a single atomic layer. This extreme precision in fabrication, necessary to obtain the unique device characteristics, together with the large number of layers and the complexity of the structure, makes this laser the most impressive demonstration of the capabilities offered by bandgap engineering. The speedy transfer of QCLs out of the research laboratories into practical fabrication has been stimulated by the variety of performances that these devices can deliver in the fields as diverse as environmental monitoring, health, safety, security, defense, medical diagnostics, electronic counter measures, and chemical sensing [3-5]. Within this last area (chemical detection and monitoring) a big improvement is expected since the combination of QCLs and recent gas sensor developments promises to deliver new levels of spectroscopic performance in terms of detection sensitivity and selectivity.

Nuclear Technology & Radiation Protection
Scientific paper
UDC: 66.088:502.1
DOI: 10.2298/NTRP0902075R

Authors' address:
Department of Microelectronics and Engineering Physics
Faculty of Electrical Engineering, University of Belgrade,
73, Bulevar Kralja Aleksandra, 11120 Belgrade, Serbia

E-mail address of corresponding author:
radovanovic@etf.bg.ac.rs (J. Radovanović)

In particular, the terahertz frequency range, which occupies the gap between the traditional mid-infrared and mm-wave portions of the electromagnetic spectrum is promising for many attractive ways of usage as it contains the characteristic absorption features of organic crystals (such as explosives, not detectable by common means but having very characteristic absorption lines in the THz-range), biologically significant chemical compounds (such as some components of bacteria), and low-energy protein conformational modes. Sensors operating at these wavelengths possess many interesting properties, including the ability to penetrate common non-metallic containers, packaging and clothing materials. Furthermore, these technologies are foreseen as a tool for addressing security gaps for protection against terrorism in infrastructures where high through-put screening of individuals or items is required. Preliminary measurements have shown that rapid identification, or fingerprinting, of explosive is achievable in 10 ms at extrapolated sensitivities in the sub-part per billion range [6].

In this paper, we consider the structural parameter optimization of the active region of GaAs/$Al_xGa_{1-x}As$ based mid-infrared quantum cascade laser, with the goal of maximizing its output properties, in particular the optical gain, at characteristic wavelengths, suitable for detection of pollutant gasses in the ambient air. In mid-infrared devices, the desired emission wavelength imposes the required separations between the active laser energy states, while the spacing between the lower laser level and the ground state is set by the longitudinal optical (LO) phonon energy (which facilitates the population inversion by allowing the fast emptying of the lower laser state by means of non-radiative transitions). However, the parameters of interest in the calculation of the optical gain, such as the population inversion and the transition matrix element, still depend, via the wave functions, on the potential profile which may be varied to optimize the performance of the structure. The relationships between these parameters are very complex, making the optimization process difficult and demanding. A large spatial overlap between the electronic wave functions of the lasing states increases the dipole matrix element which enhances the optical transition, but also results in the reduction of the electron-longitudinal optical phonon scattering time. Since these two quantities influence the gain in an opposite manner, a balance has to be found to ensure the proper operation of the device, and it becomes apparent that a carefully selected optimization technique should be employed. One of the best tools for the systematic search of free parameter space is the genetic algorithm (GA) [7, 8] for global optimization whose inherent parallelism in generating and processing the trial solutions allows dealing with such complex optimization problems.

Upon obtaining a gain-maximized structure emitting at desired wavelength, we introduce a strong external magnetic field to tune the laser output properties and to extend the applicability of the given structure to the detection of additional compounds, absorbing at wavelengths close to the initial one. The magnetic field is applied perpendicularly to the epitaxial layers, thus causing two-dimensional continuous energy subbands to split into series of discrete Landau levels (LLs). This affects all the relevant relaxation processes in the structure and consequently the lifetime of carriers in the upper laser level. Since the arrangement of Landau levels depends strongly on the magnitude of the magnetic field, this enables one to control the population inversion in the active region, and hence the optical gain [9-12]. In addition, strong effects of band non-parabolicity alter the lasing wavelength at magnetic fields which maximize the gain, thus providing means for adjusting the output radiation properties and changing the target compound for detection. The complete procedure was illustrated by performing numerical calculations for GaAs/$Al_xGa_{1-x}As$ based quantum cascade laser structures designed to emit at specified wavelengths in the mid-infrared part of the spectrum.

THEORETICAL CONSIDERATIONS

The active region of the QCL structure under consideration comprises three coupled quantum wells (QWs) biased by an external electric field K, as displayed in fig. 1. In the absence of the magnetic field this system has three energy states, *i. e.*, subbands (n = 1, 2, 3), and the laser transition occurs between subbands n = = 3 and n = 2. The energy difference between E_2 and E_1 should match the LO-phonon energy in order to ensure fast depopulation of the lower state of the laser transition via resonant optical-phonon emission.

This active region is surrounded by suitable emitter/collector regions in the form of superlattices, designed as Bragg refectors, which inject electrons into the state n = 3 on one side, and allow for rapid ex-

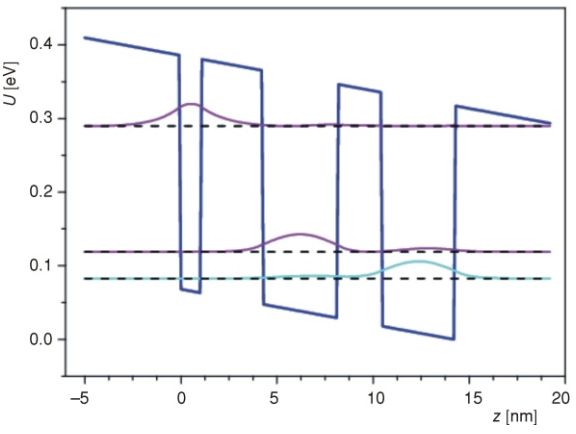

Figure 1. The conduction band diagram of the active region of a QCL

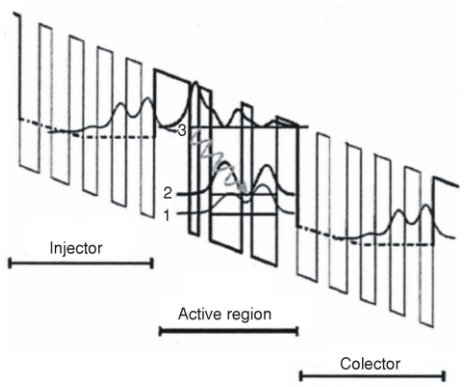

Figure 2. A schematic diagram of one and a half period of QCL, which consists of an active region and suitable injector/collector layers

traction of carriers from the lowest subband $n = 1$, on the other side (fig. 2). These two mechanisms are responsible for achieving population inversion between subbands E_3 and E_2.

In the usual operating regime (without the external magnetic field), the electronic subbands from fig. 1, within the parabolic approximation have free particle-like energy dispersion in the direction parallel to the QW planes: $E_n \quad \hbar^2 k_\parallel^2 / 2m^*$, where m^* is the effective mass, and $k_\parallel$ is the in-plane wave vector. The non-radiative lifetime for the state $|3, k_\parallel$ is limited by electron-LO-phonon scattering into two lower subbands of the active region, and the optical gain may be described by the following expression

$$g_{3,2} \quad \frac{e^2}{2n\varepsilon_0 \omega m_0^2 c} \int_0^\infty F_{3,2} P_{3,2}^2 \delta(E_3 \quad E_2 \quad \hbar\omega) d(k_\parallel^2) \tag{1}$$

where n is the refractive index, ε_0 is the vacuum dielectric permittivity, c is the speed of light in vacuum, $F_{3,2}$ stands for the difference of Fermi-Dirac functions for the initial and the final state, while $P_{3,2}$ is the momentum matrix element.

When the structure is subjected to a strong magnetic feld B in the direction of the growth axis, continuous subbands $E_n(k_\parallel)$ transform into series of individual (strictly discrete) states at energies $E_{n,l} \quad E_n \quad (l \quad 1/2)\hbar\omega_c$, where $l = 0, 1, 2, ...$ is the Landau index and $\omega_c \quad eB/m^*$ is the cyclotron frequency. The variation of the magnetic field B influences the configuration (energy spacings) of the discrete states, and hence the probabilities for emission of LO phonon and the optical gain. The values of B which give rise to the resonant LO phonon emission (and in consequence, the dramatic reduction of the gain) are found by solving the equation: $E_{3,0} \quad E_{n,l} \quad \hbar\omega_{LO}$ (with $n = 1, 2$), where $\hbar\omega_{LO}$ is the LO phonon energy.

Optical transitions in this system are allowed only between the states with the same value of the Landau index, *i. e.* $(i, l) \quad (f, l)$. The fractional absorption (or, if it comes out to be negative, the gain) on transitions corresponding to the lasing energy, *i. e.* (2, *l*) (3, *l*) reads [10-12]

$$A_{2,1 \quad 3,l} \quad \frac{e^3 \pi B}{\hbar n \varepsilon_0} \frac{d_{2,3}^2}{\lambda} \delta(E_{3,l} \quad E_{2,l} \quad \hbar\omega) F_{2,l;3,l} \tag{2}$$

$F_{2,l;3,l}$ is the difference of Fermi-Dirac functions for the initial and the final state, and $d_{if} \quad \eta_i |z| \eta_f$ is the transition matrix element (with η_i and η_f denoting the z-dependent parts of the wavefunctions). Using the expression for the electron areal density in the state (n, l), *i. e.* $N_{n,l} \quad eB/(\pi\hbar) F_{FD}(E_{n,l})$ and summing over all LLs, we get the total gain on all transitions between LLs belonging to subbands $n = 3$ and $n = 2$ of the QCL active region [10-12]

$$g_{2,3} \quad \frac{2e^2 \pi^2}{n\varepsilon_0} \frac{d_{2,3}^2}{\lambda} \delta(E_{3,l} \quad E_{2,l} \quad \hbar\omega) \quad (N_{S3} \quad N_{S2}) \tag{3}$$

To determine the population inversion $N_{S3} - N_{S2}$, on which the gain depends, one has to find the electron distribution over all the states in the active region. This is obtained by solving the system of rate equations, which describe the change in level population as the difference between the rate at which the carriers arrive and the rate at which they leave. The exact form of the rate equations used in this work is presented in detail in references [10, 11].

Numerical results

The need for numerical and simulation tools in studying QCLs stems from the fact that simple analytical expressions clearly cannot describe the important details of the QCL dynamics. In this work we have selected the genetic algorithm as a method of choice for establishing the conditions for optimal laser performance [7]. This algorithm belongs to the so-called evolutionary computing – one of the essential spheres of artificial intelligence. Clearly, this technique is inspired by the theory of evolution, where problems are solved by selecting "the most capable" solution which is then allowed to survive [7]. GA begins with a set of solutions called population which is used as a basis for generating another set of "offsprings" with the best possible characteristics (defined by the value of the objective, *i. e.* the fitness function). This process is repeated until some predefined criterion is met (this could be, *e. g.* the total number of populations generated or the improvement in the fittest solution). The performance of the algorithm is influenced mainly by settings associated with the recombination (or crossover) and the mutation probability. The crossover represents a set of rules for creating new offsprings ("children") from parent data. On the other hand, mutations

introduce random changes in the offsprings resulting from the crossover and are intended to prevent the falling of all the solutions into a local optimum. One of the most important phases in the implementation of any GA algorithm is the selection of a formal fitness function, which should be defined so to encompass all the goals of optimization. This can present quite a complicated task, depending on the optimization problem, and usually a few different definitions of fitness need to be tried out. Here, the objective is to optimize the optical gain at the selected wavelength, hence the fitness function is taken in the following form

$$F \quad \frac{g(B \quad 0)}{\{(E_3 \quad E_2 \quad E_{SO_2})^2 \quad \Theta^2\}\{(E_2 \quad E_1 \quad \hbar\omega_{LO})^2 \quad \Theta^2\}} \tag{4}$$

where the term in the denominator favours achieving specified emission wavelength and the LO-phonon resonance. In this example, we have chosen to optimize the structure for emission at $\lambda \quad 7.3$ m, which corresponds to a characteristic line in the spectrum of sulphur-dioxide. In addition, Θ is a non-zero constant, which ensures that F is strongly driven towards the resonance in the course of optimization [8], while remaining finite at the exact resonance, and g is the optical gain in the absence of the magnetic field, given by eq. (1).

The role of the GA is to simultaneously vary all six free parameters on which the fitness function (4) depends (the barriers height and the thicknesses of all the inner layers), while searching for the optimal solution, and this procedure has resulted in the structure presented in fig. 1. The obtained structural parameters for this QCL active region read: 1.1 nm, 3.2 nm, 3.9 nm, 2.3 nm, 3.8 nm (for well and barrier widths, respectively, going from left to right) and $U_b = 0.3175$ eV(the barrier height), which corresponds to aluminum mole fraction of 38%, so the structure may be realized by GaAs/$Al_{0.38}Ga_{0.62}As$. The material parameters used in the calculation are: $m^* = 0.665\, m_0$ (m_0 is the free electron mass), $n = 3.3$, and the conduction band discontinuity between GaAs and AlAs is $\Delta E_c = 0.8355$ eV. The applied electric field in the z-direction is $K = 48$ kV/cm, and the minima of energy subbands are at $E_1(k_\parallel \quad 0) \quad 0.0828$ eV, $E_2(k_\parallel \quad 0) \quad 0.1188$ eV, and $E_3(k_\parallel \quad 0) \quad 0.2896$ eV, as presented in fig. 1, together with the corresponding wavefunctions. The calculated optical gain per unit of the injection current in this case reads $g = 0.00127$ cm^2/kA.

When non-parabolicity is included, the 2-D subbands $E_n(k_\parallel \quad 0) \quad \hbar^2 k_\parallel^2 / 2m^*$ split, in a strong external magnetic field, into series of discrete LLs, the energies of which are given by [13]

$$E_{n,l} \quad E_n(k_\parallel \quad 0) \quad (l \quad 1/2)\hbar eB/m_{\parallel n}(E_{n0})$$
$$1/8[(8l^2 \quad 8l \quad 5)\alpha_1' \quad (l^2 \quad l \quad 1)\beta_1'](\hbar eB/m^*)^2$$

The in-plane electron effective mass is here calculated as $m_\parallel(E_{n0}) \quad m^*[1 \quad (2\alpha_1' \quad \beta_1')E_{n0}]$, (this provides the best agreement with the experimental results [12]), where the non-parabolicity parameters α_1' and β_1' are evaluated according to ref. [13]. It is evident that the realistic effects of band non-parabolicity influence the energy separation between the levels relevant for the radiative transition, *i. e.* the lasing wavelength becomes dependent on the magnetic field. This allows for the shift of the emission wavelength by variations of the magnetic field. The idea behind this analysis is to enable the detection of multiple compounds absorbing at similar wavelengths by the same QCL active region design, by tuning the laser levels with the external field.

The LO phonon emission rate on the transitions between the initial state and the final state $E_i \quad E_{n_i,l_i}$ and the final state $E_f \quad E_{n_f,l_f}$ is given by [14]

$$W_{LO}(E_i,E_f) \quad \frac{e^2\omega_{LO}}{\pi\varepsilon_0\varepsilon_p}\delta(E_{n_i,l_i} \quad E_{n_f,l_f} \quad \hbar\omega_{LO})$$
$$\int_0^\infty q_\parallel \left|F^2(q_\parallel,l_i,l_f)\right|^2 dq_\parallel \quad \int_0^\infty \frac{P^2(q_z)}{q_\parallel^2 \quad q_z^2}\mathrm{d}q_z[n(\hbar\omega_{LO}) \quad 1] \tag{5}$$

where $P \quad \int_0^d \eta_i^* \sin(q_z z)\eta_f \mathrm{d}z$. Here d denotes the length of the confining region in the z-direction, and q_z is the z-projection of the phonon wavevector $q \quad (q_z, q_\parallel)$, while $\left|F(q_\parallel,l_i,l_f)\right|$ is the lateral overlap integral. The constant ε_p in eq. (5) is calculated as $\varepsilon_p^{-1} \quad \varepsilon_\infty^{-1} \quad \varepsilon_s^{-1}$, where ε_∞ and ε_s are the high-frequency and static permittivity, respectively, while $n(\hbar\omega_{LO}) \quad [\exp(\hbar\omega_{LO}/k_BT) \quad 1]^{-1}$ is the equilibrium population of optical phonons. In addition to LO phonons, we have also included the acoustic phonon emission in the model, and the corresponding relaxation rate is given by [14, 15]

$$W_{AC}(E_i,E_f) \quad \frac{\alpha_{AC}}{\pi\hbar}\left(\frac{E_i \quad E_f}{\hbar v_L}\right)^2 \frac{1}{1 \quad \exp\left(\frac{E_i \quad E_f}{k_BT}\right)}$$
$$\int_0^{q_{z\max}} \left|P(q_z)\right|^2 \left|F(q_{\parallel 0},l_i,l_f)\right|^2 \mathrm{d}q_z \tag{6}$$

where $\alpha_{AC} \quad \Xi^2 / c_L$, Ξ is the deformation potential, c_L – the elastic constant associated with acoustic vibrations, $q_{z_{max}} = [(E_i - E_f)/\hbar v_L]$, $q_{\parallel 0} = [q_{z_{max}}^2 \quad q_z^2]^{1/2}$, and v_L – the longitudinal phonon velocity. Numerical parameters used in the calculations are: $\varepsilon_\infty = 10.67$, $\varepsilon_s = 12.51$, $\Xi = = 6.7$ eV, $c_L = 1.2\ 10^{11}$ N/m^2, $v_L = 4.7\ 10^3$ m/s, and T = = 77 K.

The total relaxation rate for transitions from the ground LL of the third subband (into which the majority of carriers are injected) into the two sets of LLs of the two lower subbands is shown in fig. 3, for the magnetic fields in the range of 20 T to 60 T. Such high values of the magnetic field are necessary to provide suf-

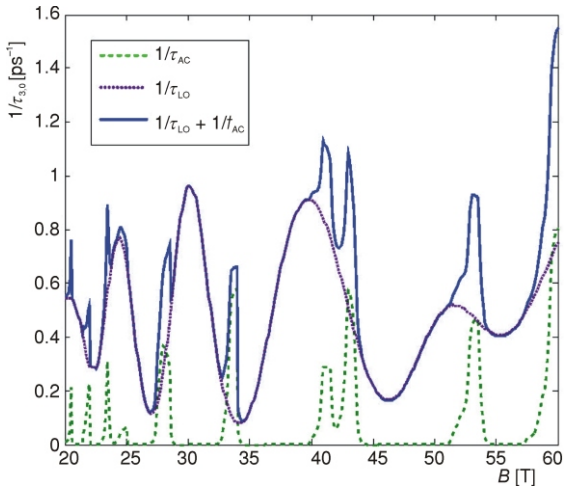

Figure 3. The total electron relaxation rate due to the emission of optical and acoustic phonons as a function of the magnetic field, for transitions from the state (3, 0) into LLs belonging to the two lower subbands

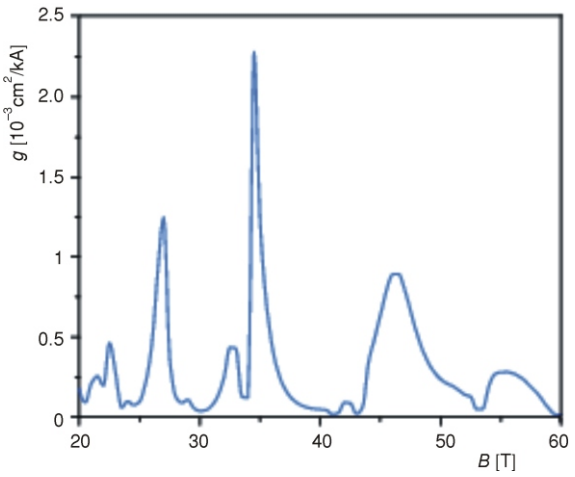

Figure 5. The optical gain (per unit of the injection current) as a function of the applied magnetic field at $T = 300$ K

ficient changes in the lasing energy, so that the device may be utilized effectively for the detection of several compounds absorbing at similar wavelenghts. The oscillations of the relaxation rate with B are very pronounced, and prominent peaks are found at the values of the magnetic field which satisfy the resonance conditions for LO phonon emission. Conversely, when the arrangement of LLs is such that there is no level situated at $\hbar\omega_{LO}$ below the state (3, 0), this type of scattering is inhibited, and therefore the lifetime of the upper laser state is increased. The influence of acoustic-phonon emission is characterized with relatively small relaxation rates, and becomes significant only at the values of the magnetic field where LO phonon scattering is inhibited (*e. g.*, around 27.5 T and 34.5 T).

Assuming a constant current injection, the modulation of lifetimes of all the states in the system results

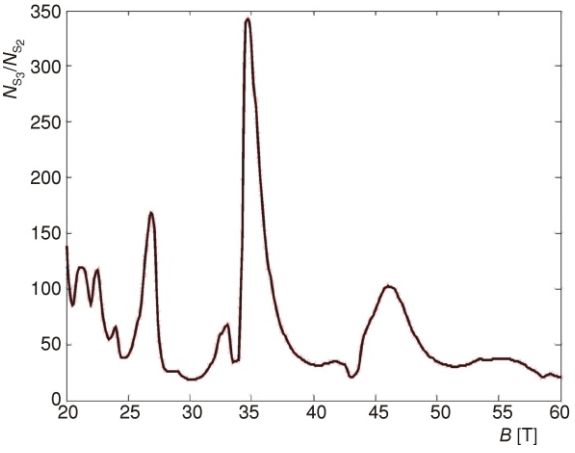

Figure 4. The ratio of the total electron areal densities, in all LLs of the third and second subband as a function of the magnetic field

in either a suppression or an enhancement of population inversion between states (3, 0) and (2, 0), as shown in fig. 4 and therefore also in the modulation of the optical gain, fig. 5.

The highest peak of the gain is obtained at B = = 34.5 T, in which case the electron relaxation from state (3, 0) is suppressed because there is no lower state with the energy around $E_{3,0}$ $\hbar\omega_{LO}$. Quite a different situation occurs at a field of $B = 30$ T, where the configuration of relevant electronic states leads to the maximally enhanced relaxation rate from the (3,0) state.

The lasing energy obtained in case of the maximal optical gain (at 34.5 T) corresponds to a characteristic absorption line in the spectrum of HNO_3, (λ = = 7.52 m, *i. e.* the wavenumber $k = 1330$ cm^{-1}). The next peak of the gain is reached at the magnetic field value of $B = 46$ T and the energy between the laser levels in this case reads $E_{3,0} - E_{2,0} = 163.8$ meV, which coincides with the line at $k = 1320$ cm^{-1} in the spectrum of methane (CH_4). Finally, a smaller local maximum at $B = 55$ T gives the emission wavelengths of $\lambda = 7.66$ m which are suitable for absorption at $k = 1306$ cm^{-1} line in the spectrum of NO_2.

As the final point, we should note that throughout the above considerations we have assumed that the energy relaxation in the injector/collector is not sensitive to the magnetic field. This is likely to be a reasonable approximation since these regions consist of a multitude of the extended states with small energy separation [9].

CONCLUSIONS

Tunable access to the broad range of wavelengths, excellent power and wavelength stability, compact dimensions, convenient modulation mechanisms, high continuous-wave output power, and

steady progress towards high temperature operation imply many strategic potential applications of QCLs, such as inorganic and biological material spectroscopy, imaging, free-space communications, and medical diagnostics. We have presented a method for systematic optimization of a quantum cascade laser active region, based on the use of genetic algorithm. The method aims at obtaining a gain-maximized structure, designed to emit radiation at specified wavelengths suitable for the detection of pollutant compounds in the atmosphere. The external magnetic field is used to tune the output properties and to extend the applicability of the QCL to the detection of additional compounds, absorbing at wavelengths close to the initial one. The numerical results are presented for the structure designed for the emission at λ 7.3 m, corresponding to a characteristic line in the spectrum of sulphur-dioxide. However, the procedure can easily be modified for other characteristic wavelengths (pollutant gasses) of interest, simply by changing the objective function for optimization.

ACKNOWLEDGEMENT

This work has been supported by the Ministry of Science and Technological Development (Republic of Serbia), through the project no. 141006 and by NATO Collaborative Linkage Grant (reference CBP. EAP.CLG 983316).

REFERENCES

[1] Gmachl, C., Capasso, F., Sivco, D. L., Cho, A. Y, Recent Progress in Quantum Cascade Lasers and Applications, *Rep. Prog. Phys., 64* (2001), 11, pp. 1553-1601

[2] Faist, J., Capasso, F., Sivco, D. L, Sirtori, C., Hutchinson, A. L., Cho, A. Y., Quantum Cascade Laser, *Science, 264* (1994), 5158, pp. 553-556

[3] Kosterev, A., Tittel, F., Chemical Sensors Based on Quantum Cascade Lasers, *IEEE J. Quantum Electron., 38* (2002), 6, pp. 582-591

[4] Wysocki, G., Lewicki, R., Curl, R. F., Tittel, F. K., Diehl, L., Capasso, F., Troccoli, M., Hofler, G., Bour, D., Corzine, S., Maulini, R., Giovannini, M., Faist, J., Widely Tunable Mode-Hop Free Externa Lcavity Quantum Cascade Lasers for High Resolution Spectroscopy and Chemical Sensing, *Appl. Phys. B, 92* (2008), 3, pp. 305–311

[5] McManus, J. B., McManns, J. B., Shorter, J. H., Nelson, D. D., Zahniser, M. S., Glenn, D. E., McGovern, R. M., Pulsed Quantum Cascade Laser Instrument with Compact Design for Rapid, High Sensitivity Measurements of Trace Gases in Air, *Appl. Phys. B, 92* (2008), 3, pp. 387–392

[6] Normand, E., Howieson, I., McCulloch, M., Black P., Quantum Cascade Laser (QCL) Based Sensor for the Detection of Explosive Compounds, *Proc. SPIE, 6402* (2006), 64020G

[7] Whitley, D., An Overview of Evolutionary Algorithms, Practical Issues and Common Pitfalls, *Inf. Software Technol., 43* (2001), 14, pp. 817–831

[8] Radovanović, J., Milanović, V., Ikonić, Z., Indjin, D., Application of the Generic Algorithm to the Optimized Design of Semimagnetic Semiconductor-Based Spin-Filters, *J. Phys. D: Appl. Phys., 40* (2007), 17, pp. 5066-5070

[9] Becker, C., Sirtori, C., Drachenko, O., Rylkov, V., Leotin, J., GaAs Quantum Box Cascade Lasers, *Appl. Phys. Lett., 81* (2002), 16, pp. 2941-2943

[10] Radovanović, J., Mirčetić, A., Milanović, V., Ikonić, Z., Indjin, D., Harrison, P., Kelsall, R. W., Influence of the Active Region Design on Output Characteristics of GaAs/AlGaAs Quantum Cascade Lasers in a Strong Magnetic Field, *Semicon. Sci. Technol., 21* (2006), 3, pp. 215-220

[11] Radovanović, J., Milanović, V., Ikonić, Z., Indjin, D., Harrison, P., Electron-Phonon Relaxation Rates and Optical Gain in a Quantum Cascade Laser in a Magnetic Field, *J. Appl. Phys., 97* (2005), 10, pp. 103109-103113

[12] Radovanović, J., Milanović, V., Ikonić, Z., Indjin, D., Control of Optical Gain in the Active Region of Quantum Cascade Laser by Strong Perpendicular Magnetic Field, *Material Science Forum, 494* (2005), pp. 31-36

[13] Ekenberg, U., Nonparabolicity Effects in a Quantum Well, Sublevel Shift, Parallel Mass, and Landau Levels, *Phys. Rev. B, 40* (1989), 11, pp. 7714-7726

[14] Turley, P. J., Teitsworth, S. W., Bose, B. K., Theory of Localized Phonon Modes and Their Effects on Electron Tunneling in Double-Barrier Structures, *J. Appl. Phys., 72* (1992), 6, pp. 2356-2366

[15] Sun, G., Khurgin, J., Optically Pumped Four-Level Infrared Laser Based on Intersubband Transitions in Multiple Quantum Wells, Feasibility Study, *IEEE J. Quantum Electron., 29* (1993), 4, pp. 1104-1111

Јелена РАДОВАНОВИЋ, Витомир МИЛАНОВИЋ

КВАНТНИ КАСКАДНИ ЛАСЕР: ПРИМЕНЕ У ХЕМИЈСКОЈ ДЕТЕКЦИЈИ И МОНИТОРИНГУ ЖИВОТНЕ СРЕДИНЕ

У овом раду разматрана је оптимизација структурних параметара активне области квантног каскадног ласера базираног на GaAs, у циљу максимизирања оптичког појачања на карактеристичним таласним дужинама које су најпогодније за детекцију штетних гасова присутних у амбијенту, као што су SO_2, HNO_3, и NH_3, путем директне апсорпције. Поступак се заснива на примени сложених алата за глобалну оптимизацију, као што је генетски алгоритам. Један од важних циљева је проширење опсега применљивости појединачне активне области на детекцију више једињења која апсорбују на блиским таласним дужинама, и то се постиже увођењем јаког магнетног поља у правцу нормалном на епитаксијалне слојеве. Ово поље доводи до цепања континуалних дводимензионалних енергетских подзона на серије дискретних Ландауових нивоа. Пошто распоред Ландауових нивоа значајно зависи од јачине магнетног поља, то омогућава контролисање степена инверзне насељености нивоа у активној области, а самим тим и оптичког појачања. Штавише, изражени ефекти зонске непараболичности резултују благим променама таласне дужине емитованог зрачења при вредностима магнетног поља када је појачање максимално и на тај начин омогућавају фино подешавање особина излазног зрачења и промену циљног једињења за детекцију. Нумерички резултати су приказани за квантни каскадни ласер дизајниран за емитовање на специфичним таласним дужинама у средњој инфрацрвеној области спектра.

Кључне речи: квантни каскадни ласер, електрон-фонон интеракције, електронска структура, глобална оптимизација, унутарзонски прелази